MRI signatures of cortical microstructure in human development align with oligodendrocyte cell-type expression

Sila Genc[1,2,3], Gareth Ball[2,4], Maxime Chamberland[1,5], Erika P Raven[1,6], Chantal MW Tax[1,7], Isobel Ward[1,8], Joseph YM Yang[2,3,4], Marco Palombo[1], Derek K Jones[1]

1. Cardiff University Brain Research Imaging Centre (CUBRIC), Cardiff University, Cardiff, United Kingdom
2. Developmental Imaging, Clinical Sciences, Murdoch Children's Research Institute, Parkville, Victoria, Australia
3. Neuroscience Advanced Clinical Imaging Service (NACIS), Department of Neurosurgery, The Royal Children's Hospital, Parkville, Victoria, Australia
4. Department of Paediatrics, University of Melbourne, Parkville, Victoria, Australia
5. Eindhoven University of Technology, Department of Mathematics and Computer Science, Eindhoven, The Netherlands
6. Center for Biomedical Imaging, Department of Radiology, New York University Grossman School of Medicine, New York, USA
7. Image Sciences Institute, University Medical Center Utrecht, Utrecht, The Netherlands
8. Data and Analysis for Social Care and Health, Office for National Statistics, Newport, United Kingdom

Abstract

Neuroanatomical changes to the cortex during adolescence have been well documented using MRI, revealing ongoing cortical thinning and volume loss. Recent advances in MRI hardware and new biophysical models of tissue informed by diffusion MRI data hold promise for identifying the cellular changes driving these morphological observations. Using ultra-strong gradient MRI, this study quantified cortical neurite and soma microstructure in typically developing youth. Cortical neurite signal fraction, attributed to neuronal and glial processes, increased with age (mean $R^2_{fneurite}$=.53, p<3.3e-11, 11.91% increase over age), while apparent soma radius decreased (mean R^2_{Rsoma}=.48, p<4.4e-10, 1% decrease over age) across domain-specific networks. Analyses of two independent post-mortem datasets revealed that genes increasing in expression through adolescence were significantly enriched in cortical oligodendrocytes and Layer 5-6 neurons. Here, we show spatial and temporal alignment of oligodendrocyte cell-type gene expression with neurite and soma microstructural changes, suggesting that ongoing cortical myelination processes drive adolescent cortical development.

1. Context

Over the last two decades, magnetic resonance imaging (MRI) has provided invaluable insights into the developing brain, revealing ongoing cortical thinning and cortical volume loss throughout adolescence (Mills et al., 2016; Tamnes et al., 2017). However, the underlying cellular processes driving these changes are less understood. Cortical cytoarchitecture can be broadly categorised into neurites (e.g., axons, dendrites, and glial processes) and soma (e.g., neuronal, and glial cell bodies). Traditionally, synaptic pruning has been considered the primary driver of developmental changes in cortical morphology (Huttenlocher, 1979). Recent evidence, however, suggests that myelin encroachment into the grey/white matter boundary may also contribute to changes in MR contrast typically used for volumetrics, such as T_1 (Natu et al., 2019). Developmental patterns of cortical myelination have been elucidated using magnetization transfer (MT) imaging (Paquola et al., 2019), and indirectly using T1w/T2w ratio (Grydeland et al., 2019). Despite these advances, how microstructural changes – specifically neurite and soma properties – contribute to these distinct morphological changes remains unclear.

Diffusion-weighted MRI (dMRI) is the main non-invasive MRI technique capable of probing the tissue microstructure, orders of magnitude smaller than the typical millimetre image resolution of structural MRI (Le Bihan et al., 2001). This microstructural imaging method is highly sensitive to the magnitude and direction of water diffusing within brain tissue. By employing biophysical models, it is possible to infer microscopic properties of different tissues, such as neurite signal fraction in the brain's white matter (Alexander et al., 2019; Zhang et al., 2012). In comparison with white matter, grey matter cytoarchitecture, broadly categorized into neurites (e.g., elongated structures such as axons, dendrites and glial processes) and soma (e.g., spherical structures such as neuronal and glial cell-bodies) is more locally complex, requiring extensions of the standard models of microstructure developed for studying the white matter. Recent hardware (Fan et al., 2022; Jones et al., 2018) and biophysical modelling (Jelescu et al., 2022; Palombo et al., 2020; Tax et al., 2020) developments have enabled diffusion-weighted microstructural quantification of soma and neurite components in the cortex in vivo. The Soma and Neurite Density Imaging (SANDI; Palombo et al. (2020)), is robust, reliable (Genc et al., 2021), clinically feasible for sufficiently short diffusion times (Schiavi et al., 2023) and has been validated in ex vivo data (Ianuş et al., 2022).

SANDI is a biophysical tissue model that estimates the diffusion-weighted signal contribution from three distinct compartments: intra-neurite, intra-soma, and extracellular space. For each imaging voxel, a signal fraction will be estimated for each of the three compartments, such that they sum to 1. In the cortical grey matter, there is a higher proportion of soma (neuronal and glial cell bodies) to neurites, leading to a higher soma signal fraction. These signal fractions vary around tissue boundaries, with higher extracellular signal fraction around the cortical surface due to partial voluming with CSF. Overall, these compartment-specific signal fractions are relative, and comparing these trends over age are potentially meaningful to deduce the compartments that are contributing most to age-related changes in cortical development.

Here, we examine cortical microstructural development in a sample of children and adolescents using ultra-strong gradient dMRI to identify specific changes in neurite and soma properties with age. To identify potential cellular substrates, we analyse developmental patterns of neurite and soma microstructure alongside contemporaneous trajectories of cortical cell-type specific gene expression measured in the developing cortex using data from two independent, post-mortem databases. We reveal key developmental patterns in cortical neurite and soma architecture, highlighting the contribution of active and ongoing cortical myelination processes to the macroscale changes observed in the cortex during adolescence.

2. Results

We apply a framework for cortical microstructure and cell-type specific gene expression analysis (Fig 1) to evaluate the cellular properties underpinning human cortical microstructural development.

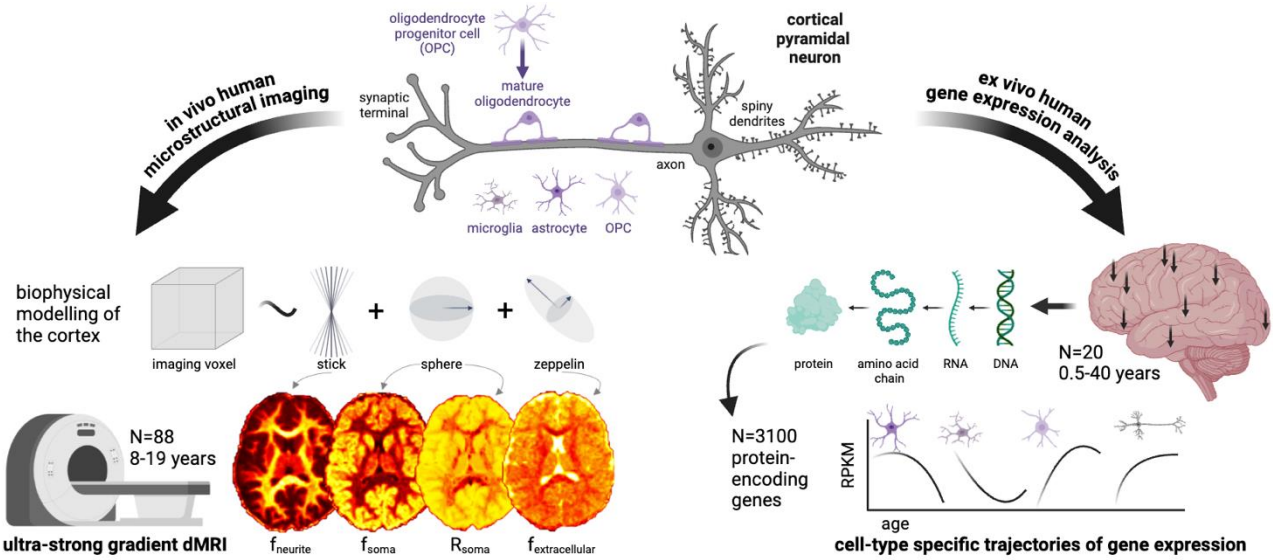

Figure 1: Framework for cortical microstructure and gene expression analysis. This study employs a biophysical model of cortical neurite and soma microstructure using ultra-strong gradient dMRI (Jones et al., 2018) data collected from 88 children and adolescents aged 8-19 years. Representative maps of neurite signal fraction ($f_{neurite}$), soma signal fraction (f_{soma}), apparent soma radius (R_{soma}, μm) and extracellular signal fraction ($f_{extracellular}$) are shown for one 8-year-old female participant. We also analyse two human gene expression datasets (Colantuoni et al., 2011; Li et al., 2018) to estimate cell-type specific and spatial (where arrows on brain render indicate a subset of regions sampled) gene expression profiles and examine their concordance with developmental patterns of cortical microstructure.

2.1. Cortical microstructure and morphology in domain-specific networks

First, we studied the repeatability of cortical microstructural estimates from the SANDI model in a sample of 6 healthy adults scanned over 5 sessions. Intra-class coefficients (ICCs) for neurite signal fraction ($f_{neurite}$), soma signal fraction (f_{soma}) and extracellular signal fraction ($f_{extracellular}$) were very high (Fig 2c) across seven domain-specific networks (mean ICC=.97, all p<.001). Apparent soma radius (R_{soma}, in μm) showed lower repeatability on average (mean ICC=.92) with lower mean repeatability driven by the limbic network.

We then studied age-related patterns of cortical microstructure and morphology in a sample of 88 typically developing children and adolescents aged 8-19 years (Table S2). Cortical $f_{neurite}$ and intracellular volume fraction (v_{ic}; derived from the NODDI model, Zhang et al. (2012)) increased with age across all cortical networks (mean $R^2_{fneurite}$=.53, all networks p<3.3e-11; mean R^2_{vic}=.46, all networks p<1.6e-9) (Fig 2d, Fig S1). Orientation dispersion index (ODI; derived from the NODDI model, Zhang et al. (2012)) also increased with age across all studied networks (mean R^2_{odi}=.42, all networks p<1.9e-5). In contrast, we observed decreasing R_{soma} with age across all

networks (mean R^2_{Rsoma}=.48, all networks p<4.4e-10) and f_{soma} decreased with age in the dorsal attention (R^2_{fsoma}=.12), limbic (R^2_{fsoma}=.09) and somatomotor (R^2_{fsoma}=.23), networks (all p<.002). $f_{extracellular}$ decreased in the default mode (R^2_{fe}=.12), limbic (R^2_{fe}=.21) and visual (R^2_{fe}=.09) networks (all p<.004). DTI metrics revealed decreasing FA with age across all networks apart from the limbic network (mean R^2 = .27, p<2.1e-5), decreasing MD in the limbic network, β= -.42, [-.62, -.22], p=8.8e-5, and increasing MD in the somatomotor network, β= .34, [.13, .55], p=.002.

Consistent with established developmental patterns, cortical thickness and grey matter volume decreased with age (Fig 2b). The strength of these associations varied across brain networks (see Fig S1 and Table S2). Specifically, cortical thickness exhibited age-related decline in the default mode, β= -.59 [-.77, -.41], dorsal attention, β= -.40 [-.61, -.19], somatomotor, β= -.40 [-.60, -.19], and visual, β= -.61 [-.78, -.43], networks (all p<.001). Similarly, grey matter volume decreased with age in the default mode, β= -.37 [-.55, -.20], dorsal attention, β= -.34 [-.54, -.15], and visual β= -.29 [-.47, -.11], networks (all p<.002). Cortical surface area did not show significant age-related differences. The magnitude and direction of age effects across all microstructural and morphological measures are shown in Figure S1.

Sex differences in brain structure have been well reported, with pubertal onset playing a critical role in initiating developmental changes to morphology (Vijayakumar et al., 2018) and microstructure (Tamnes et al., 2018). We found that grey matter volume and surface area were higher in males than females (p<.005) across all brain networks (Figure S2), following known patterns of larger brain volume in males. We observed sex differences in only two microstructural measures, R_{soma} and fractional anisotropy (FA; derived from the diffusion tensor at b=1200 s/mm^2), in the visual network (Fig S2, S3). Females had higher R_{soma}, β= -.57 [-.91, -.24], p=.001, and lower FA, β= .55, [.18, .92], p=.004, compared to males. We observed a pubertal stage by sex interaction on f_{soma}, where males had lower soma signal fraction in early puberty, β= .73 [.28, 1.18], p=.002, which stabilised in late puberty. Males had lower $f_{extracellular}$ throughout puberty β= -.74 [-1.18, -.31], p=.001. To further demonstrate developmental differences in the visual network we built an age prediction model (see supplementary section 8.3.2 and Figure S10) which showed that R_{soma} provided the most accurate age-prediction (cross-validated R^2=.58). Feature importance revealed top-ranking regions represent cortical endpoints of developmentally sensitive tracts, identified through tractography, such as the posterior corpus callosum, cingulum, and inferior longitudinal fasciculus (Fig S10d).

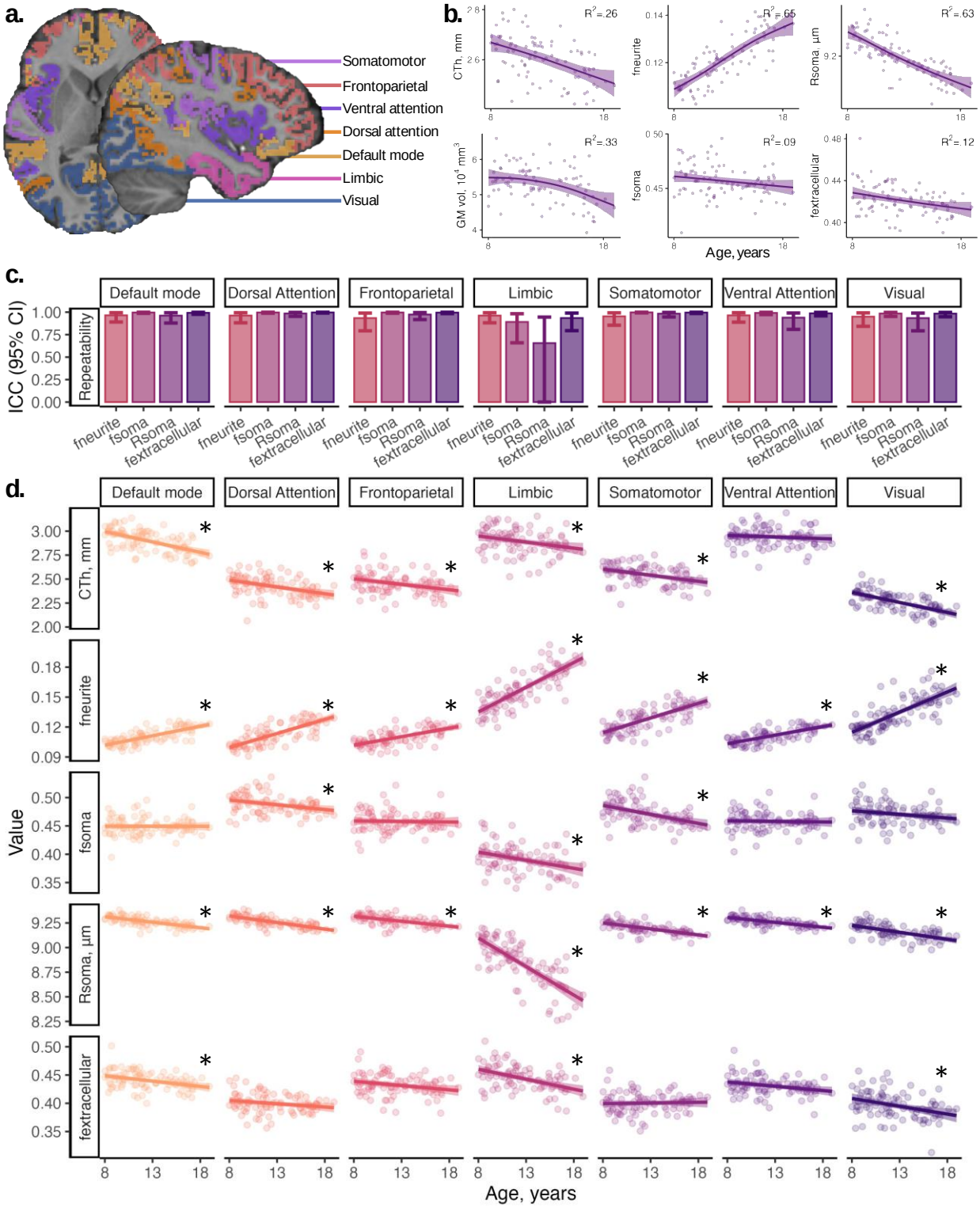

Figure 2: Developmental patterns of MRI-derived cortical morphology and microstructure: (a) regions in atlas used to derive domain-specific networks (Yeo et al., 2011) overlaid on a representative participant; (b) developmental patterns of cortical morphology and microstructure averaged across the cortical ribbon; (c) demonstration of high repeatability of SANDI measures in six adults scanned over 5 time-points within two weeks; (d) network-wide patterns of microstructure and morphology, indicating age-related increases in neurite fraction and reductions in cortical thickness, apparent soma radius, soma fraction and extracellular fraction. Significant age relationships ($p<.005$)

are annotated (*). Abbreviations: CTh: cortical thickness, in mm; $f_{extracellular}$: extracellular signal fraction; $f_{neurite}$: neurite signal fraction; f_{soma}: soma signal fraction; GM: grey matter; ICC: intra-class coefficient; R_{soma}: apparent soma radius, in μm.

2.2. Contemporaneous gene expression trajectories

Using n=214 post-mortem tissue samples from the dorsolateral prefrontal cortex (DLFPC; BrainCloud; Colantuoni et al. (2011)), we identified n=2057 genes with differential expression over the lifespan (0.5 – 72 years; $p_{FDR}<0.05$). We validated this selection in an independent RNA-seq dataset (PsychENCODE; Li et al. (2018); n=20), identifying n=467 (22.7%) genes with significant age-associations in both datasets (age-genes; Supp Info).

We identified sets of differentially expressed genes across 7 cortical cell-types (see Methods). Mean trajectories of gene expression across ages 0 and 30 years, averaged within each cell-type, are shown as standardized curves in Figure 3 for PsychENCODE (Fig 3a) and BrainCloud (Fig 3b) datasets. Developmental profiles from the DLPFC were visualised, to allow for clearer comparisons of cell-type specific trends over age between cohorts. Non-normalized gene expression curves for PsychENCODE are presented in Figure S4 to aid in interpreting relative differences in gene expression magnitudes. Among genes expressed in excitatory neuronal populations and oligodendrocytes, mean expression levels increased with age. In contrast, genes expressed in inhibitory neurons showed no age-related variation. Genes expressed in endothelial cells, astrocytes, microglia and OPCs, exhibited a decrease in mean gene expression with age. Overall, microglial gene expression (mean log_2RPKM =1.96) was lower compared to astrocytes (mean log_2RPKM =3.70), oligodendrocytes (mean log_2RPKM =3.11), OPCs (mean log_2RPKM =3.01), excitatory neurons (mean log_2RPKM =4.15) and inhibitory neurons (mean log_2RPKM =2.94). To validate our bulk-tissue findings in an independent dataset, we took advantage of a recent single-cell RNA atlas of pre- and postnatal brain development (Velmeshev et al., 2023). Using these data, we identified a set of cell-specific genes with an onset of expression in childhood (>4 years) followed by a rapid increase through adolescence and into adulthood (n=534 genes). Most of these genes were expressed by oligodendrocytes (n=349; Figure S12), confirming our findings from bulk-tissue data.

We confirmed the enrichment of cell-types identified in the age-related genes identified using bulk-tissue data using an independent cell-type specific expression analysis (CSEA). Significant enrichment of age-genes (n=467) was observed in cortical oligodendrocytes, oligodendrocyte progenitors, and Layer 5-6 neurons (Fig S5).

These genes were prominently expressed across developmental stages in childhood adolescence, and young adulthood (Fig S6, Fig 3c). The number (Fig 3d) and proportion (Fig 3e) of age-related genes expressed by oligodendrocytes increased significantly in adolescence and young adulthood (Fig 3d,e). These included genes associated with CNS (re)myelination, RCAN2 (Huang et al., 2011), GRIA3 (Kougioumtzidou et al., 2017), and the differentiation of OPCs and oligodendrocytes, PLEHA1/TAPP1 (Chen et al., 2015); AATK/AATYK (Jiang et al., 2018).

For each cell-type, we quantified the spatiotemporal patterns of gene expression using PsychENCODE data by identifying the peak growth of expression in cell-specific genes. Oligodendrocyte gene expression peaked earliest in primary motor (M1), primary visual (V1) cortices, and latest in the medial frontal (MFC) cortex (Fig S8). A notable pattern emerged in which the peak expression of oligodendrocyte genes coincided with a shift in oligodendrocyte-to-astrocyte specific expression ratio. This shift, indicating a relative increase in oligodendrocyte over astrocyte cell-type gene expression, occurred around 20 years of age in M1 and V1, and after age 25 in DLPFC, ITC and MFC (Fig 3g,h). This sequence aligns with the known earlier myelination timing in sensorimotor cortices followed by prolonged myelination in the pre-frontal cortex into the third decade of life (Grydeland et al., 2019; Paquola et al., 2019; Sydnor et al., 2021).

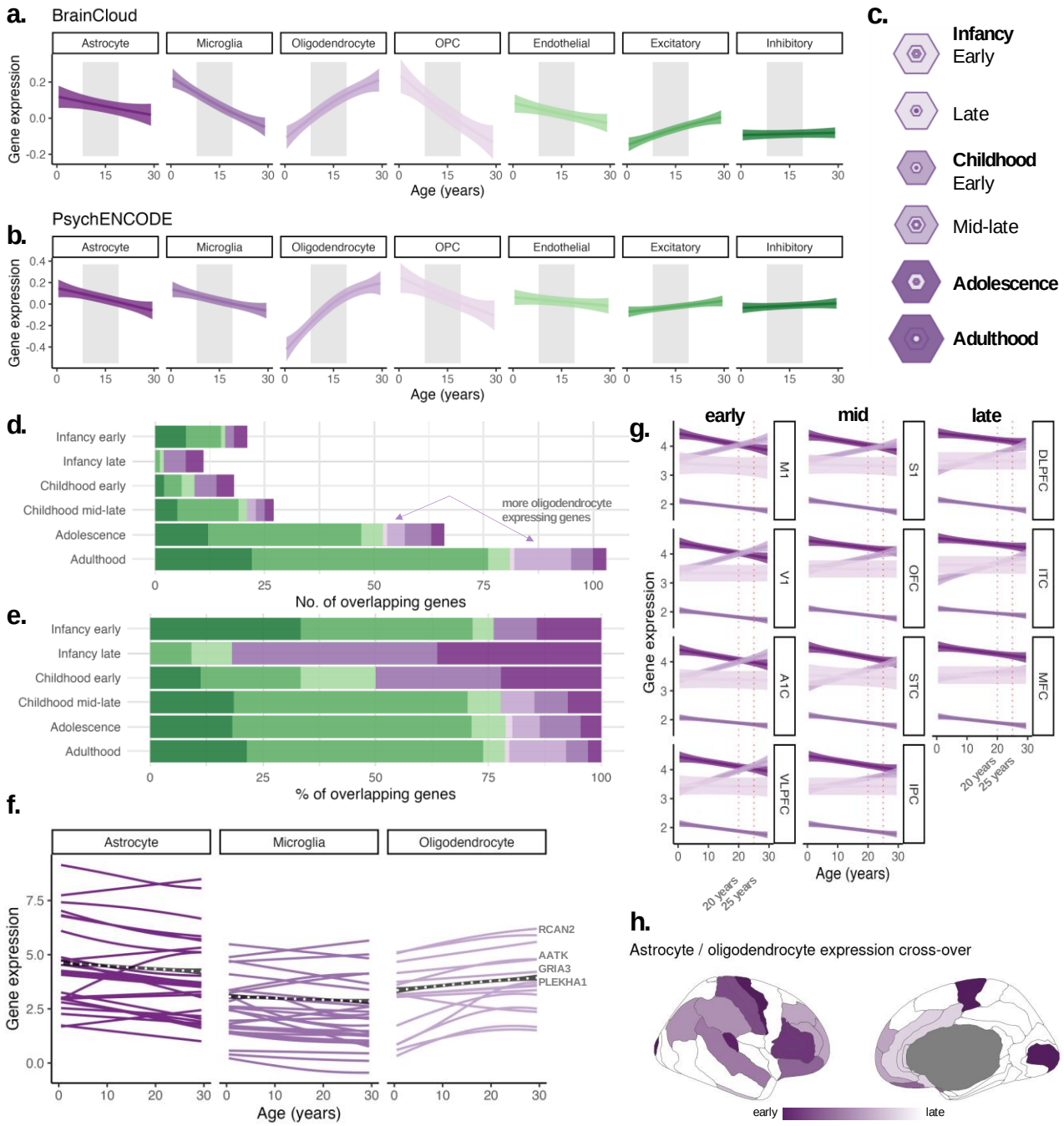

Figure 3: Developmental trajectories of cell-type specific gene expression. Data shown for samples aged 0-30 years from: (a) BrainCloud (Z-score), and (b) PsychENCODE (expressed in log_2-reads-per-kilobase of transcript per million (log_2RPKM)) datasets, demeaned to account for overall higher expression in some cell-types. Age effects were modelled in all postnatal samples to maximise sample size. Grey shaded areas highlight the age range of the microstructural imaging cohort (8-19 years) for visual comparison of developmental profiles. (c) SEA results (Xu et al., 2014) showing significant enrichment of age-related genes through adolescence and adulthood, where hexagon size scales with enrichment (overlap) of age-related genes in genes expressed by each cell type, and darker rings indicate significant associations at p_{FDR}<.001 with inner rings indicating

high cell specificity. Age-related genes overlapping postnatal developmental stages are shown as (d) total number of genes, and (e) proportion of genes, indicating an increase in neuronal, glial and oligodendrocyte-specific genes. (f) Trajectories of glial genes overlapping the SEA and our age-genes. (g) Regional shifts in the glial cell-type expression ratio (log_2RPKM) across development, with the astrocyte-to-oligodendrocyte expression ratio crossing earliest at age 20 years in primary motor and visual cortices. (h) Timing of this cross-over, with darker values indicating regions with an earlier crossing point. Note that white coloured regions are not represented in the data set.

2.3. Concordant profiles of microstructure and gene expression indicate developmental cortical myelination

To elucidate the cell-specific basis of our imaging findings, we examined neurite and soma microstructural measures in the same four frontal regions sampled in the PsychENCODE data (MFC, IFC, DLPFC, VLPFC; see Fig 4a,b) using a fine-grained parcellation of the frontal lobe. Microstructural MRI revealed regional increases in $f_{neurite}$ and decreases in R_{soma} (Fig 4c). This pattern corresponded with increased regional oligodendrocyte cell-type gene expression profiles in the same regions over the same age period (Fig 4d,e). The spatial distribution of oligodendrocyte cell-type expression was aligned with regional differences in peak growth of the neurite fraction (Fig S7). Thus, the dMRI-derived neurite signal fraction likely reflects spatiotemporal patterns of cortical myelination, matching the peak expression of oligodendrocyte-genes.

To further evaluate the concordance between in vivo MRI and ex vivo gene expression patterns, we performed numerical simulations using realistic cell counts to explain age-related patterns of the apparent soma radius. Assuming that the observed age-related slope of gene expression was proportional to the number of cells of each cell-type within an MRI voxel, we modelled cell-type composition changes based on the actual expected distribution of cell body radii within a voxel based on realistic cell counts and sizes. Our results revealed close correspondence between simulated and in vivo modelling results of R_{soma} (Fig S9), showing a 1% age-related decrease in both simulated and dMRI-derived data across 8-19 years.

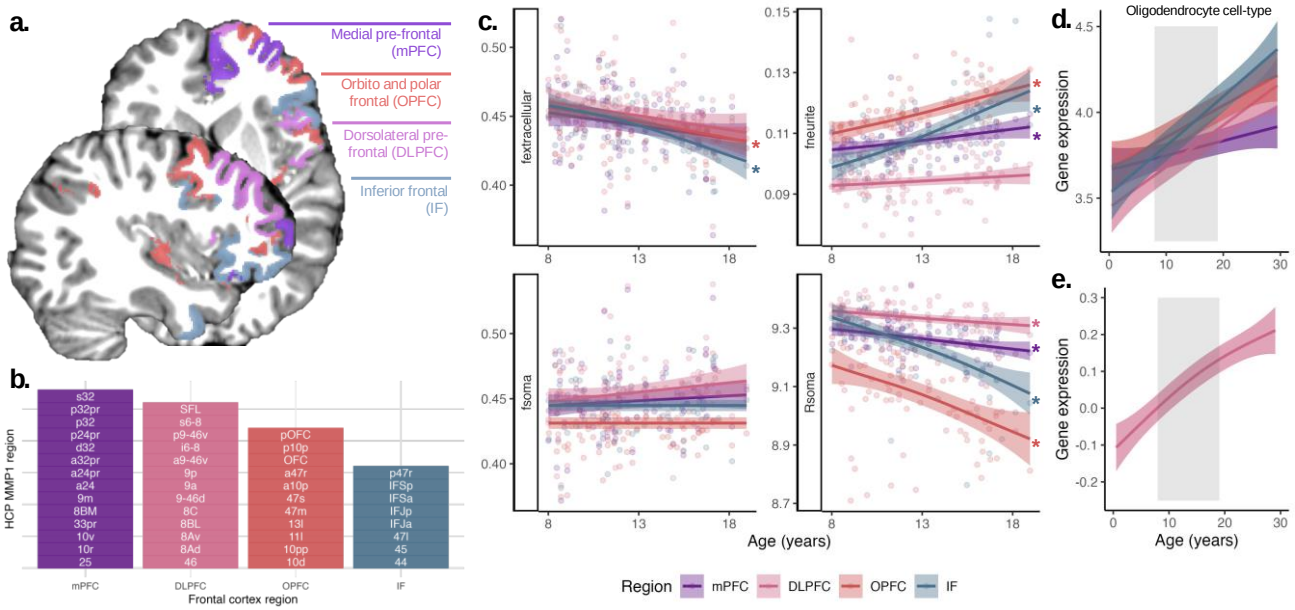

Figure 4: Regional variation of microstructure and gene expression in the frontal cortex. (a) Structural MRI-based segmentation of four frontal regions: medial pre-frontal cortex (mPFC); dorsolateral prefrontal cortex (DLPFC); orbito and polar frontal cortex (OPFC), and inferior frontal cortex (IF); (b) sub-regions from the HCP-MMP1 atlas (Glasser et al., 2016), which comprised the regions in (a); (c) age-related patterns of microstructural measures (*:p<.005); oligodendrocyte cell-type gene expression in (d) PsychENCODE data sampled in the same 4 frontal cortical regions as (a), and (e) BrainCloud data sampled in the DLPFC.

3. Discussion

We combined in vivo ultra-strong gradient dMRI with independent ex vivo gene expression analyses to map tissue microstructural architecture during human development. We now discuss each of the key findings and their implications, before summarising the strengths and limitations of our study.

Neurite Signal Fraction Increases from Childhood to Adolescence

The neurite signal fraction, $f_{neurite}$, attributed to elongated cortical structures (e.g., axons, processes), increased with age across the whole cortex, but peaked earliest in the visual and somatomotor networks, mirroring previous findings (Lynch et al., 2024). Intracortical myelination continues over adolescence (Bartzokis, 2012; Gibson et al., 2014; Grydeland et al., 2019; Natu et al., 2019; Whitaker et al., 2016), following a stereotyped sensorimotor-to-association (S-A) axis of development (Sydnor et al., 2023). Although dMRI is relatively insensitive to water within the myelin sheath itself, due to its short T_2 (D. K. Jones et al., 2013), the observed increase in $f_{neurite}$ may nevertheless reflect intra-cortical myelination. This is supported by ex vivo macaque data showing developmental increases in glial process length and complexity (Robillard et al., 2016), and an increase in the number of myelinated

axons and dendrites (Fukutomi et al., 2018), which limits water exchange and leads to a greater signal contribution from inside the neurite (Jelescu et al., 2022; Olesen et al., 2022).

Oligodendrocyte-Specific Gene Expression Increases from Childhood to Adolescence

Supporting our in vivo MRI findings, oligodendrocyte-specific gene expression increased with age (Fig 4a,b), aligning with previous observations in independent data (Paquola et al., 2019). Age-related genes were also enriched in cortical neurons (layers 5 and 6) and OPCs (Fig S6). The concordance between the human bulk-tissue gene expression analysis (Fig S5), human single-cell RNA analysis (Fig S12), and the CSEA analysis based on mouse transcriptomic profiling (Fig S6) indicates conservation of myelination processes via cortical oligodendrocytes. Oligodendrocyte cell turnover in the frontal cortex is dynamic, especially in adulthood, and 10 times higher in the cortex than in the white matter (Yeung et al., 2014). OPCs can generate myelinating oligodendrocytes in adulthood, even in fully myelinated regions (Richardson et al., 2011; Young et al., 2013). Importantly, oligodendrocyte function is not restricted to myelination, rather, they also perform many critical neuronal support functions beyond myelination (Bradl & Lassmann, 2010). Together our microstructural MRI and gene-expression findings converge towards increased cortical myelination through adolescence.

Apparent Soma Radius Decreases from Childhood to Adolescence

The dMRI-derived apparent soma radius, R_{soma}, decreased cortex-wide from childhood to adolescence. Neuronal soma are much larger than glial soma, measuring ~16μm in diameter in layers 5-6 of the adult human prefrontal cortex, whereas glial soma range in diameter from 1-11μm (Rajkowska et al., 1998). Our gene expression analysis suggests specific changes in the cellular composition of the cortex with age: decreasing expression levels for astrocyte, microglia and endothelial cell-types, and (much larger) increasing expression levels for oligodendrocyte cell-types. Glial composition in the neocortex is mostly comprised of oligodendrocytes (~75%), followed by astrocytes (~20%) and a smaller prevalence of microglia (~5%) (Pelvig et al., 2008). Assuming gene expression levels are proportional to cell number/density, our observations suggest a decrease in large-soma cells (e.g., endothelial), outweighed by a larger increase in small-soma cells (e.g., oligodendrocytes).

The estimated R_{soma} is dependent on the higher order moments of the soma radii distribution (i.e. skewdness and tailedness) within an MRI voxel (Olesen et al.,

2022). Our own simulations of R_{soma} based on known cell composition in the human brain (Keller et al., 2018) revealed a decrease in apparent soma radii with age matching our in vivo imaging observations (i.e., a 1% decrease). This would in turn lead to a reduction in the measured dMRI signal coming from water molecules fully restricted in soma, aligning with our in vivo observations of decreasing f_{soma} with age in the limbic, somatomotor, and dorsal attention networks. It is plausible that an increase in oligodendrocyte (Peters & Sethares, 2004), not astrocyte or microglial (Robillard et al., 2016), composition could concomitantly result in a smaller average soma radii and lower soma signal fraction in the cortex through adolescence to early adulthood.

Sex Differences in Microstructural Properties

Females have larger apparent soma radii than males, and f_{soma} and $f_{extracellular}$ varies with pubertal stage in the visual network (Fig S10a). Pubertal hormones can stimulate apoptosis (seen in female rat visual cortex; Nunez et al. (2002)), which could explain the lower f_{soma} as puberty progresses in females. Selective neuronal cell death with unchanged glial cell number can also occur during puberty in the medial pre-frontal cortex (Markham et al., 2007; Willing & Juraska, 2015), however we did not observe any sex or pubertal differences in microstructure of the frontal cortex.

Extracellular Signal Fraction and Myelination

In dMRI, myelin thickening can decrease the extracellular signal fraction, due to less physical space in the extracellular matrix (Jelescu et al., 2016; Derek K Jones et al., 2013). Age-related decreases in $f_{extracellular}$ were confined to the visual network and orbito-frontal and inferior frontal cortices. Comprehensive evaluation of the myelin content is warranted to confirm the contributions of intracortical myelination to developmental changes in cortical morphology (Mancini et al., 2020).

Spatiotemporal Patterns of Gene Expression

Peak oligodendrocyte cell-type gene expression progressed along the S-A axis, with earliest peaks in M1 and V1, and latest in MFC (Fig S8), mirroring spatial patterns of peak $f_{neurite}$ (Fig S7). This also coincided with a relative age-related decrease in astrocyte cell-type gene expression (Fig 4g) consistent with early-life maturation of astrocytes (Bushong et al., 2004; Cahoy et al., 2008). The S-A developmental axis describes a maturation process from lower-order, primary sensory and motor (unimodal) cortices to higher-order transmodal association cortices, which support complex neurocognitive, and socioemotional functions (Margulies et al., 2016; Sydnor

et al., 2021). Prolonged maturation of the pre-frontal cortex has been reported with lower myelin content in fronto-polar cortex compared with visual or somatomotor regions from childhood to adulthood (Miller et al., 2012) indicating later myelination timing. Within the frontal cortex, age-related patterns of microstructural neurite signal fraction and soma radius were prolonged in the MFC and DLPFC (Fig 4c-e). This reflects the value of estimating in vivo neurite signal fraction as these developmental hierarchies have been reproduced across various modalities (Burt et al., 2018; Gao et al., 2020; Satterthwaite et al., 2014; Sydnor et al., 2021; Vaishnavi et al., 2010; Wagstyl et al., 2015), particularly when considering the regions reaching peak maturation earliest and latest. Overall, our combined imaging genetic analyses supports the evidence of an orderly and hierarchical progression of intracortical myelination.

Implications for Cortical Thinning

A recent study showed that cortical thinning during development is associated with genes expressed predominantly in astrocytes, microglia, excitatory and inhibitory neurons (Zhou et al., 2023). We observed faster cortical thinning of default-mode and visual networks, consistent with previous studies (Ball, Seidlitz, Beare, et al., 2020; Zhou et al., 2023). Apparent thinning may be a result of the macrostructural shift in the boundary between grey matter and white matter, in this scenario due to myelin encroachment into the cortex (Mournet et al., 2020; Natu et al., 2019). The microstructural composition of the grey matter itself may be better studied by the biophysical models used here.

~~Clinical implications~~ Potential applications

Cortical morphology and myelination abnormalities are linked to various neuropsychiatric disorders (Chen et al., 2024) including schizophrenia (Alexander-Bloch et al., 2014; Wannan et al., 2019) which is characterised by deficiencies in myelination and oligodendrocyte production (Davis et al., 2003; Katsel et al., 2005). One potential future application is to quantify cortical microstructure in such clinical cohorts, especially with adaptations towards clinically feasible acquisition protocols using current state-of-the-art clinical grade 3T systems (Barakovic et al., 2024; Margoni et al., 2023; Schiavi et al., 2023), and with the recent advent of commercial systems with ultra-strong gradients (e.g., Siemens 3T Cima.X; GE 3T MAGNUS). Further strengthening this potential application, schizophrenia patients exhibit downregulation of myelination-related genes (Tkachev et al., 2003) and post-mortem studies have shown reduced oligodendrocyte density in layer 5 of dorsolateral prefrontal cortex compared to healthy controls (Kolomeets & Uranova,

2019). Additionally, young children with autism show age-related deficits in cortical T1w/T2w ratios (Chen et al., 2022). Future studies exploring these novel neuroimaging measures may provide valuable insights into cortical based abnormalities.

Strengths and limitations

Several methodological advancements have advanced the understanding of underlying compositional changes to cortical microstructure across development in our study. Our repeatability results show that SANDI-derived biophysical signal fractions are highly stable (mean ICC=.97) in a young adult population, and these values are highly concordant with recently reported cortex-wide measurements in a subset of younger adults (Lee et al., 2024). Using in vivo microstructural imaging with ultra-strong gradients (G_{max}=300 mT/m; Jones et al. (2018)), we achieved sensitivity to micrometer-level imaging contrast by maximising SNR and minimising the effect of water exchange (Raven et al., 2023). Although we used a specialised system, recent advancements have enabled these measurements on more accessible, lower-gradient strength MRI systems (e.g. $G_{max}\geq$80mT/m; Schiavi et al. (2023)). Combined with two ex vivo gene expression data sets sampled from the human brain, we provide compelling evidence in favour of a framework for monitoring intra-cortical cellular composition in vivo. Further work should evaluate in vivo imaging acquisition techniques and models that account for water exchange, which can influence biophysical modelling of grey matter compartments.

Our observation of oligodendrocyte-specific gene expression increasing towards adulthood indicates the value of imaging a broader age range of young adults to fully assess trajectories of in vivo microstructural properties. It is also important to recognise that gene expression patterns do not necessarily correlate with cellular density. Histopathological confirmation is needed to verify cell size and density with biophysical signal fractions, as well as their relevancy to functional gene expression patterns.

Overall, our study provides novel *in vivo* evidence of distinct developmental differences in neurite and soma architecture, aligning with cell-type specific gene expression patterns observed in *ex vivo* human data. This provides a window into the role of intracortical myelination through adolescence, and how it shapes the developmental patterns of cortical microstructure in vivo.

4. Methods

4.1. Imaging set

4.1.1. Participant characteristics

We included a sample of 88 typically developing children aged 8-19 years recruited as part of the Cardiff University Brain Research Imaging Centre (CUBRIC) Kids study. The study was approved by the School of Psychology ethics committee at Cardiff University. Participants and their parents/guardians were recruited via public outreach events. Written informed consent was obtained from the primary caregiver of each child participating in the study, and adolescents aged 16-19 years also provided written consent. Children were excluded from the study if they had non-removable metal implants or reported history of a major head injury or epilepsy.

We administered a survey to parents of all participants, and to children aged 11-19 years. The Strengths and Difficulties Questionnaire (SDQ) was used to assess emotional/behavioural difficulties (Goodman, 1997). The Pubertal Development Scale (Petersen et al., 1988) was used to determine pubertal stage (PDSS; Shirtcliff et al. (2009)). Additionally, we measured each child's height and weight to calculate their Body-Mass index (BMI) (kg/m^2).

All children and adolescents underwent in-person training to prepare them for the MRI procedure using a dedicated mock MRI scanner. This protocol was 15-30 minutes long, and designed to familiarise them to the scanner environment, to minimize head motion during the scan. All procedures were completed in accordance with the Declaration of Helsinki.

Table 1: Characteristics of in vivo imaging cohort.

	Summary statistics			Age relationship*	
Measure	**Mean**	**SD**	**Range**	**R^2**	***p-value***
Age, years†	12.56	2.94	8.0 - 19.0		
Pubertal stage (PDSS)†	2.89	1.50	1 - 5	.72	<.001
SDQ, total score†	6.45	3.90	0 - 19	.01	.60
Body mass index, kg/m^2‡	19.29	3.25	13.7 - 29.2	.25	<.001
FSIQˆ	108	12.6	86 - 145		

† Full sample: N=88 (42 males, 46 females)
‡ Subsample: N=79 (40 males, 39 females)
ˆ Subsample: N=48 (23 males, 25 females)
*Age relationships determined by linear regression.

4.1.2. Acquisition and processing

Discovery data: Participants aged 8-19 years (N=88, mean age=12.6 years, 46 female) underwent MRI on a 3T Siemens Connectom system with ultra-strong (300 mT/m) gradients. Structural T_1-weighted (voxel-size=1x1x1mm^3; TE/TR=2/2300 ms) and multi-shell dMRI (TE/TR=59/3000 ms; voxel-size=2x2x2 mm^3; Δ = 23.3 ms, δ = 7 ms, b-values = 0 (14 vols), 500, 1200(30 dirs), 2400, 4000, 6000 (60 dirs) s/mm^2) data were acquired. Data were acquired in an anterior-posterior (AP) phase-encoding direction, with one additional PA volume. The total acquisition time (across four acquisition blocks) was 16 min 14 s.

Repeatability data: Six healthy adults aged 24-30 years (3 female) were scanned five times in the span of two weeks (Koller et al., 2021) on the same Siemens Connectom system. Multi-shell dMRI data were collected as above, with an additional 20 diffusion directions acquired at b=200 s/ mm^2.

Pre-processing of dMRI data followed steps interfacing tools such as FSL (Smith et al., 2004), MRtrix3 (Tournier et al., 2019), and ANTS (Avants et al., 2011) as reported previously (Genc et al., 2020). Briefly, this included denoising, and correction for drift, motion, eddy, and susceptibility-induced distortions, Gibbs ringing artefact, bias field, and gradient non-uniformities. For each subject, the soma and neurite density imaging (SANDI) compartment model was fitted (Palombo et al., 2020) to dMRI data using the SANDI Matlab Toolbox v1.0, publicly available at https://github.com/palombom/SANDI-Matlab-Toolbox-v1.0, to compute whole brain maps of neurite, soma and extracellular signal fraction ($f_{neurite}$, f_{soma}, $f_{extracellular}$ = 1 - $f_{neurite}$ - f_{soma}); the soma radius (R_{soma}, in μm); and the extracellular and intra-neurite axial diffusivities (D_e and D_{in}, respectively, in μm^2/ms) (Fig 1). To put our results in context with previous studies, the neurite orientation dispersion and density imaging (NODDI) model (Zhang et al., 2012) was fitted to all b-values using the NODDI Matlab toolbox, publicly available at http://mig.cs.ucl.ac.uk/index.php?n=Tutorial.NODDImatlab , to estimate the intra-cellular volume fraction (v_{ic}) and orientation dispersion (OD) and diffusion tensor imaging

(DTI) metrics were estimated using the b=1200 s/mm^2 shell (Fractional anisotropy (FA); mean diffusivity (MD, in s/mm^2).

T1-weighted data were processed using FreeSurfer version 6.0 (http://surfer.nmr.mgh.harvard.edu) and post-processed to obtain network-level (N=7 ROIs; Yeo et al. (2011)) and fine-grained cortical parcellations (N=360, HCP-MMP1; (Glasser et al., 2016)). The network-level atlas derivation is detailed in Genc et al. (2024). Briefly, we co-registered the Yeo functional atlas in MNI space to each individual subject's space, to obtain seven functionally relevant cortical canonical networks (visual, somatomotor, dorsal attention, ventral attention, limbic, frontoparietal, default mode network). We chose a functional atlas due to the limitations of structural atlases in capturing fine-grained microstructural variations, enabling better insights into developmental patterns of neural activity and connectivity (Fotiadis et al., 2024). Follow-up analyses using fine-grained HCP-MMP1 parcellations in visual and frontal cortices were performed based on a priori hypotheses of earlier maturation of visual (Natu et al., 2019) and later maturation of frontal (Robillard et al., 2016) cortices, as well as for comparison with gene expression data sampled from multiple regions in the frontal cortex. Morphological measures including cortical thickness (CTh, mm), surface area (SA, mm^2), and grey matter volume (GMvol, mm^3) were computed at the whole brain, and parcel level. The analysis framework is detailed in Figure 1 and networks studied are depicted in Fig 2a.

4.2. Cortical gene expression set

Pre-processed, batch-corrected and normalised microarray and bulk RNA-seq data from postmortem human tissue samples were obtained from the BrainCloud (Colantuoni et al., 2011) (n=214; aged 6mo – 78.2y; 144 male; postmortem interval [PMI] = 29.96 [15.28]; RNA integrity [RIN] = 8.14 [0.83]) and PsychENCODE (n=20; 6mo-40y; 10 male; PMI = 17.85 [6.75]; RIN = 8.45 [0.79]) projects, respectively (Li et al., 2018). The cortical regions sampled are summarised in Table S1, alongside the approximate concordant Yeo7 parcel. Tissue was collected after obtaining parental or next of kin consent and with approval by the institutional review boards at the Yale University School of Medicine, the National Institutes of Health, and at each institution from which tissue specimens were obtained. Tissue processing is detailed elsewhere (Ball, Seidlitz, O'Muircheartaigh, et al., 2020; Li et al., 2018). Gene expression for PsychENCODE was measured as rates per kilobase of transcript per million mapped (RPKM). Gene expression for Braincloud was preprocessed and

normalized following data cleaning and regressing out technical variability (see https://www.ncbi.nlm.nih.gov/geo/query/acc.cgi?acc=GSE30272).

Genes were initially filtered to include only protein-coding genes expressed in cortical cell types (n=3100, Ball, Seidlitz, O'Muircheartaigh, et al. (2020)). Using a database of single-cell RNA-seq studies, we identified genes differentially expressed across major cortical cell types (excitatory and inhibitory neurons, oligodendrocytes, oligodendrocyte precursor cells [OPCs], microglia, astrocytes, and endothelial cells (Ball, Seidlitz, Beare, et al., 2020)).

4.3. Statistical analyses

4.3.1. In vivo imaging

For the repeatability analysis, the intra-class correlation coefficient (ICC; two-way random effects, absolute agreement) was computed for assessment of test-re-test repeatability for SANDI and DTI metrics using the 'psych' package in R. Lower and upper estimates of each ICC represent the bounds of the 95% confidence interval (CI).

We used linear regression to test for main effects of age and sex, puberty, and sex by puberty interactions. To identify the most parsimonious model and to avoid over-fitting, we used the Akaike Information Criterion (AIC) (Akaike, 1974), selecting the model with the lowest AIC. Individual general linear models were used to determine age-related differences in cortical thickness and microstructural measures in all seven Yeo networks. Evidence for an association was deemed statistically significant when $p < .005$ (Benjamin et al., 2018). Results from linear models are presented as the normalized coefficient of variation (β) and the corresponding 95% confidence interval [lower bound, upper bound]. We also report the adjusted correlation coefficient of the full model (R^2).

To identify important regions that contribute to age-related differences in all the studied microstructural measures, we performed age-prediction using a random forest (RF) regressor (5-fold cross-validation) for age prediction with PyCaret (www.pycaret.org). We chose a RF model due their ability to model nonlinear relationships, reduced risk of overfitting, and interpretability of feature importance. Specifically, the depth at which a feature appears as a decision node in a tree provides insight into its relative significance for predicting the target variable (i.e., age). This allows us to assess the relative contribution of features (i.e., average

signal fraction in each HCPMMP1 parcel) to age prediction. For each microstructural measure, we randomly split the data into training and validation sets using an 80-20 ratio (total N=88: 70 training; 18 testing). Then, we performed feature scaling to ensure that all input variables (for each HCPMMP1 ROI) were on a similar scale prior to model fitting. The performance of the model was evaluated on the validation dataset. Finally, the features with the largest weight coefficients were extracted to identify specific cortical regions where variance in cortical microstructure was associated with age-related changes.

4.3.2. Gene expression profiles

To identify genes differentially expressed over age (p_{FDR}<.05), we modelled age-related changes in normalised expression in all available postnatal tissue samples using nonlinear generalised additive models with thin plate splines (k=5) (Wood, 2003) in R.

BrainCloud

The relationship between normalised gene expression and age was modelled with a nonlinear general additive model (GAM) using a penalised thin-plate spline with a maximum 5 knots:

M1a. gam(expression ~
1 + s(age, k=5, bs='tp')

Note that the available BrainCloud data are already preprocessed to remove variance due to batch and sample effects (see https://www.ncbi.nlm.nih.gov/geo/query/acc.cgi?acc=GSE30272).

PsychENCODE

We repeated the above models, now with a measure of RNA integrity (RIN) as a confounder, and gene expression defined as $\log_2$(RPKM). First, we included region as an additional factor to account for spatial variation across the cortex and included donor ID as a random effect to account for repeated samples from the same specimen.

M2a. gam(expression ~
1 + s(age, k=5, bs='tp', by=region, id=1)

+ RIN + sex + region + s(sample, bs='re'), data = data))

Then, we analysed data only in the DLPFC, for comparison with the BrainCloud geneset.

M2a. gam(expression(DLPFC) ~
1 + s(age, k=5, bs='tp')
+ RIN + sex + s(sample, bs='re'), data = data))

We calculated measures of goodness of fit using Akaike Information Criterion (AIC) and Bayesian Information Criterion (BIC) for all gene models.

Using a set of independent single-cell RNA studies of the human cortex (see Ball, Seidlitz et al. (2020) for details), we identified genes exhibiting differential expression across various cortical cells-types, including excitatory neurons, inhibitory neurons, oligodendrocytes, microglia, astrocytes, and endothelial cells. We then compiled gene lists for each cell-type, comprising genes that are both differentially expressed by that cell-type, and uniquely expressed by that cell-type. Mean trajectories across all cortical regions sampled were computed for each cell-type.

After identifying age-related genes, we entered our list to an independent cell-type specific expression analysis (CSEA; Xu et al. (2014)) to elucidate: 1) if genes were enriched for specific cell-types, and 2) in which developmental period was gene expression highest.

4.3.3. Simulations

We performed numerical simulations using realistic cell counts to explain the observed trends in R_{soma} derived from in vivo dMRI data. We modelled the variability in cell body sizes within an MRI voxel by generating distributions of radii for microglia, astrocytes, oligodendrocytes, neurons, and endothelial cells. For each cell-type, we assumed the observed age-related slope of gene expression was proportional to the number of cells within an MRI voxel. Based on realistic cell counts outlined in Keller et al. (2018), we set the number of cells in mm^3 as follows: N_{micro} = 6,500; N_{astro} = 15,700; N_{oligo} = 12,500; N_{neuro} = 92,000; N_{endo} = Nneuro*.35 (Ventura-Antunes et al., 2022). For each cell type, we generated random samples of radii based on the specified cell counts assuming a Gaussian distribution with cell-type specific baseline mean and standard deviation: microglia = 2.0±0.5 μm;

astrocytes and oligodendrocytes = 5.5±1.5 μm; neurons = 8.0±2.0 μm for neurons and 9.0±0.5 μm for endothelial. The resulting radii were concatenated to form a comprehensive distribution and the MR apparent soma radius R_{soma} estimated as $\left(\frac{R^5}{R^3}\right)^{1/2}$ as per Olesen et al. (2022).

5. Data Availability

Original datasets are accessible through the original publications, including the MICRA (Koller et al., 2021) neuroimaging repeatability dataset (osf.io/z3mkn/), PsychENCODE (http://resource.psychencode.org/) and BrainCloud (https://www.ncbi.nlm.nih.gov/projects/gap/cgi-bin/study.cgi?study_id=phs000417.v2.p1). Developmental MRI data are not available due to privacy concerns, however derived data supporting the findings of the imaging analyses are available from the corresponding author upon reasonable request.

6. Code Availability

Code for gene expression analysis will be made available at github.com/garedaba/puberty-genes. TractSeg is available at github.com/MIC-DKFZ/TractSeg. MRtrix is available at www.mrtrix.org.

7. Acknowledgements

The authors would like to thank the families that participated in this study for their generous contributions. We would also like to thank Umesh Rudrapatna and John Evans for their assistance with acquisition protocols and Greg Parker and Simona Schiavi for assistance with MRI processing. Figure 1 was created with BioRender.com with elements from Macrovector via freepik.

The imaging data were acquired at the UK National Facility for In Vivo MR Imaging of Human Tissue Microstructure funded by the EPSRC (grant EP/M029778/1), and The Wolfson Foundation. SG and JYMY are supported by the Royal Children's Hospital Foundation (RCHF 2022-1402). GB is supported by a National Health and Medical Research Council Investigator Grant (1194497). EPR is supported by NICHD at NIH (F32HD103313). CMWT is supported by a Veni grant (17331) from the Dutch Research Council (NWO) and the Wellcome Trust (215944/Z/19/Z). MP is supported by a UKRI Future Leaders Fellowship MR/T020296/2. DKJ is supported by

a Wellcome Trust Investigator Award (096646/Z/11/Z) and a Wellcome Trust Strategic Award (104943/Z/14/Z).

8. Author contributions

SG, GB, MP and DKJ conceptualized the problem. SG, ER and IW acquired the developmental MRI data. SG, MC and MP analyzed the MRI data. SG, GB and MC performed statistical analyses. DKJ supervised and raised funding for this project. SG wrote the original draft of the manuscript. All authors reviewed and edited the manuscript.

9. Competing interests

The authors declare no competing interests.

10. References

Akaike, H. (1974). A new look at the statistical model identification. *IEEE Transactions on Automatic Control*, *19*(6), 716-723. https://doi.org/10.1109/TAC.1974.1100705

Alexander, D. C., Dyrby, T. B., Nilsson, M., & Zhang, H. (2019). Imaging brain microstructure with diffusion MRI: practicality and applications. *NMR in Biomedicine*, *32*(4), e3841. https://doi.org/https://doi.org/10.1002/nbm.3841

Alexander-Bloch, A. F., Reiss, P. T., Rapoport, J., McAdams, H., Giedd, J. N., Bullmore, E. T., & Gogtay, N. (2014). Abnormal cortical growth in schizophrenia targets normative modules of synchronized development. *Biol Psychiatry*, *76*(6), 438-446.

Avants, B. B., Tustison, N. J., Song, G., Cook, P. A., Klein, A., & Gee, J. C. (2011). A reproducible evaluation of ANTs similarity metric performance in brain image registration. *NeuroImage*, *54*(3), 2033-2044.

Ball, G., Seidlitz, J., Beare, R., & Seal, M. L. (2020). Cortical remodelling in childhood is associated with genes enriched for neurodevelopmental disorders. *NeuroImage*, *215*, 116803. https://doi.org/10.1016/j.neuroimage.2020.116803

Ball, G., Seidlitz, J., O'Muircheartaigh, J., Dimitrova, R., Fenchel, D., Makropoulos, A., Christiaens, D., Schuh, A., Passerat-Palmbach, J., Hutter, J., Cordero-Grande, L., Hughes, E., Price, A., Hajnal, J. V., Rueckert, D., Robinson, E. C., & Edwards, A. D. (2020). Cortical morphology at birth reflects spatiotemporal patterns of gene expression in the fetal human brain. *PLOS Biology*, *18*(11), e3000976. https://doi.org/10.1371/journal.pbio.3000976

Barakovic, M., Weigel, M., Cagol, A., Schaedelin, S., Galbusera, R., Lu, P.-J., Chen, X., Melie-Garcia, L., Ocampo-Pineda, M., Bahn, E., Stadelmann, C., Palombo, M., Kappos, L., Kuhle, J., Magon, S., & Granziera, C. (2024). A novel imaging marker of cortical "cellularity" in multiple sclerosis patients. *Scientific Reports*, *14*(1), 9848. https://doi.org/10.1038/s41598-024-60497-6

Bartzokis, G. (2012). Neuroglialpharmacology: Myelination as a shared mechanism of action of psychotropic treatments. *Neuropharmacology*, *62*(7), 2137-2153. https://doi.org/https://doi.org/10.1016/j.neuropharm.2012.01.015

Benjamin, D. J., Berger, J. O., Johannesson, M., Nosek, B. A., Wagenmakers, E. J., Berk, R., Bollen, K. A., Brembs, B., Brown, L., Camerer, C., Cesarini, D., Chambers, C. D., Clyde, M., Cook, T. D., De Boeck, P., Dienes, Z., Dreber, A., Easwaran, K., Efferson, C., Fehr, E., Fidler, F., Field, A. P., Forster, M., George, E. I., Gonzalez, R., Goodman, S., Green, E., Green, D. P., Greenwald, A. G., Hadfield, J. D., Hedges, L. V., Held, L., Hua Ho, T., Hoijtink, H., Hruschka, D. J., Imai, K., Imbens, G., Ioannidis, J. P. A., Jeon, M., Jones, J. H., Kirchler, M., Laibson, D., List, J., Little, R., Lupia, A., Machery, E., Maxwell, S. E., McCarthy, M., Moore, D. A., Morgan, S. L., Munafó, M., Nakagawa, S., Nyhan, B., Parker, T. H., Pericchi, L., Perugini, M., Rouder, J., Rousseau, J., Savalei, V., Schönbrodt, F. D., Sellke, T., Sinclair, B., Tingley, D., Van Zandt, T., Vazire, S., Watts, D. J., Winship, C., Wolpert, R. L., Xie, Y., Young, C., Zinman, J., & Johnson, V. E. (2018). Redefine statistical significance. *Nature Human Behaviour*, *2*(1), 6-10. https://doi.org/10.1038/s41562-017-0189-z

Bradl, M., & Lassmann, H. (2010). Oligodendrocytes: biology and pathology. *Acta neuropathologica*, *119*, 37-53.

Burt, J. B., Demirtaş, M., Eckner, W. J., Navejar, N. M., Ji, J. L., Martin, W. J., Bernacchia, A., Anticevic, A., & Murray, J. D. (2018). Hierarchy of transcriptomic specialization across human cortex captured by structural neuroimaging topography. *Nat Neurosci*, *21*(9), 1251-1259. https://doi.org/10.1038/s41593-018-0195-0

Bushong, E. A., Martone, M. E., & Ellisman, M. H. (2004). Maturation of astrocyte morphology and the establishment of astrocyte domains during postnatal hippocampal development. *International Journal of Developmental Neuroscience*, *22*(2), 73-86. https://doi.org/https://doi.org/10.1016/j.ijdevneu.2003.12.008

Cahoy, J. D., Emery, B., Kaushal, A., Foo, L. C., Zamanian, J. L., Christopherson, K. S., Xing, Y., Lubischer, J. L., Krieg, P. A., Krupenko, S. A., Thompson, W. J., & Barres, B. A. (2008). A transcriptome database for astrocytes, neurons, and oligodendrocytes: a new resource for understanding brain development and function. *J Neurosci*, *28*(1), 264-278. https://doi.org/10.1523/jneurosci.4178-07.2008

Chen, B., Linke, A., Olson, L., Kohli, J., Kinnear, M., Sereno, M., Müller, R. A., Carper, R., & Fishman, I. (2022). Cortical myelination in toddlers and preschoolers with autism spectrum disorder. *Dev Neurobiol*, *82*(3), 261-274. https://doi.org/10.1002/dneu.22874

Chen, J., Patel, Z., Liu, S., Bock, N. A., Frey, B. N., & Suh, J. S. (2024). A systematic review of abnormalities in intracortical myelin across psychiatric illnesses. *Journal of Affective Disorders Reports*, *15*, 100689. https://doi.org/https://doi.org/10.1016/j.jadr.2023.100689

Chen, Y., Mei, R., Teng, P., Yang, A., Hu, X., Zhang, Z., Qiu, M., & Zhao, X. (2015). TAPP1 inhibits the differentiation of oligodendrocyte precursor cells via suppressing the Mek/Erk pathway. *Neurosci Bull*, *31*(5), 517-526. https://doi.org/10.1007/s12264-015-1537-5

Colantuoni, C., Lipska, B. K., Ye, T., Hyde, T. M., Tao, R., Leek, J. T., Colantuoni, E. A., Elkahloun, A. G., Herman, M. M., Weinberger, D. R., & Kleinman, J. E. (2011). Temporal dynamics and genetic control of transcription in the human prefrontal cortex. *Nature*, *478*(7370), 519-523. https://doi.org/10.1038/nature10524

Davis, K. L., Stewart, D. G., Friedman, J. I., Buchsbaum, M., Harvey, P. D., Hof, P. R., Buxbaum, J., & Haroutunian, V. (2003). White Matter Changes in Schizophrenia: Evidence for Myelin-Related Dysfunction. *Archives of General Psychiatry*, *60*(5), 443-456. https://doi.org/10.1001/archpsyc.60.5.443

Fan, Q., Eichner, C., Afzali, M., Mueller, L., Tax, C. M. W., Davids, M., Mahmutovic, M., Keil, B., Bilgic, B., Setsompop, K., Lee, H. H., Tian, Q., Maffei, C., Ramos-Llordén, G., Nummenmaa, A., Witzel, T., Yendiki, A., Song, Y. Q., Huang, C. C., Lin, C. P., Weiskopf, N., Anwander, A., Jones, D. K., Rosen, B. R., Wald, L. L., & Huang, S. Y. (2022). Mapping the human connectome using diffusion MRI at 300 mT/m gradient strength: Methodological advances and scientific impact. *NeuroImage*, *254*, 118958. https://doi.org/10.1016/j.neuroimage.2022.118958

Fotiadis, P., Parkes, L., Davis, K. A., Satterthwaite, T. D., Shinohara, R. T., & Bassett, D. S. (2024). Structure–function coupling in macroscale human brain networks. *Nature reviews neuroscience*, *25*(10), 688-704. https://doi.org/10.1038/s41583-024-00846-6

Fukutomi, H., Glasser, M. F., Zhang, H., Autio, J. A., Coalson, T. S., Okada, T., Togashi, K., Van Essen, D. C., & Hayashi, T. (2018). Neurite imaging reveals microstructural variations in human cerebral cortical gray matter. *NeuroImage*, *182*, 488-499. https://doi.org/https://doi.org/10.1016/j.neuroimage.2018.02.017

Gao, R., van den Brink, R. L., Pfeffer, T., & Voytek, B. (2020). Neuronal timescales are functionally dynamic and shaped by cortical microarchitecture. *Elife*, *9*. https://doi.org/10.7554/eLife.61277

Genc, S., Chamberland, M., Koller, K., Tax, C. M. W., Zhang, H., Palombo, M., & Jones, D. K. (2021). Repeatability of Soma and Neurite Metrics in Cortical and Subcortical Grey Matter. In N. Gyori, J. Hutter, V. Nath, M. Palombo, M. Pizzolato, & F. Zhang (Eds.), *Computational Diffusion MRI* (pp. 135-145). Springer International Publishing.

Genc, S., Schiavi, S., Chamberland, M., Tax, C. M. W., Raven, E. P., Daducci, A., & Jones, D. K. (2024). Developmental differences in canonical cortical networks: insights from microstructure-informed tractography. *Network Neuroscience*, 1-48. https://doi.org/10.1162/netn_a_00378

Genc, S., Tax, C. M. W., Raven, E. P., Chamberland, M., Parker, G. D., & Jones, D. K. (2020). Impact of b-value on estimates of apparent fibre density. *Human Brain Mapping*, *41*(10), 2583-2595. https://doi.org/10.1002/hbm.24964

Gibson, E. M., Purger, D., Mount, C. W., Goldstein, A. K., Lin, G. L., Wood, L. S., Inema, I., Miller, S. E., Bieri, G., Zuchero, J. B., Barres, B. A., Woo, P. J., Vogel, H., & Monje, M. (2014). Neuronal activity promotes oligodendrogenesis and adaptive myelination in the mammalian brain. *Science*, *344*(6183), 1252304. https://doi.org/10.1126/science.1252304

Glasser, M. F., Coalson, T. S., Robinson, E. C., Hacker, C. D., Harwell, J., Yacoub, E., Ugurbil, K., Andersson, J., Beckmann, C. F., & Jenkinson, M. (2016). A multi-modal parcellation of human cerebral cortex. *Nature*, *536*(7615), 171-178.

Grydeland, H., Vértes, P. E., Váša, F., Romero-Garcia, R., Whitaker, K., Alexander-Bloch, A. F., Bjørnerud, A., Patel, A. X., Sederevičius, D., & Tamnes, C. K. (2019). Waves of maturation and senescence in micro-structural MRI markers of human cortical myelination over the lifespan. *Cerebral Cortex*, *29*(3), 1369-1381.

Huang, J. K., Jarjour, A. A., Nait Oumesmar, B., Kerninon, C., Williams, A., Krezel, W., Kagechika, H., Bauer, J., Zhao, C., Baron-Van Evercooren, A., Chambon, P., Ffrench-Constant, C., & Franklin, R. J. M. (2011). Retinoid X receptor gamma signaling accelerates CNS remyelination. *Nat Neurosci*, *14*(1), 45-53. https://doi.org/10.1038/nn.2702

Huttenlocher, P. R. (1979). Synaptic density in human frontal cortex - developmental changes and effects of aging. *Brain Res*, *163*(2), 195-205. https://doi.org/10.1016/0006-8993(79)90349-4

Ianuş, A., Carvalho, J., Fernandes, F. F., Cruz, R., Chavarrias, C., Palombo, M., & Shemesh, N. (2022). Soma and Neurite Density MRI (SANDI) of the in-vivo mouse brain and comparison with the Allen Brain Atlas. *NeuroImage*, *254*, 119135. https://doi.org/https://doi.org/10.1016/j.neuroimage.2022.119135

Jelescu, I. O., de Skowronski, A., Geffroy, F., Palombo, M., & Novikov, D. S. (2022). Neurite Exchange Imaging (NEXI): A minimal model of diffusion in gray matter with inter-compartment water exchange. *NeuroImage*, *256*, 119277. https://doi.org/https://doi.org/10.1016/j.neuroimage.2022.119277

Jelescu, I. O., Zurek, M., Winters, K. V., Veraart, J., Rajaratnam, A., Kim, N. S., Babb, J. S., Shepherd, T. M., Novikov, D. S., Kim, S. G., & Fieremans, E. (2016). In vivo quantification of demyelination and recovery using compartment-specific diffusion MRI metrics validated by electron microscopy. *NeuroImage*, *132*, 104-114. https://doi.org/https://doi.org/10.1016/j.neuroimage.2016.02.004

Jiang, C., Yang, W., Fan, Z., Teng, P., Mei, R., Yang, J., Yang, A., Qiu, M., & Zhao, X. (2018). AATYK is a Novel Regulator of Oligodendrocyte Differentiation and Myelination. *Neurosci Bull*, *34*(3), 527-533. https://doi.org/10.1007/s12264-018-0218-6

Jones, D. K., Alexander, D. C., Bowtell, R., Cercignani, M., Dell'Acqua, F., McHugh, D. J., Miller, K. L., Palombo, M., Parker, G. J. M., Rudrapatna, U. S., & Tax, C. M. W. (2018). Microstructural imaging of the human brain with a 'super-scanner': 10 key advantages of ultra-strong gradients for diffusion MRI. *NeuroImage*, *182*, 8-38. https://doi.org/10.1016/j.neuroimage.2018.05.047

Jones, D. K., Knösche, T. R., & Turner, R. (2013). White matter integrity, fiber count, and other fallacies: the do's and don'ts of diffusion MRI. *NeuroImage*, *73*, 239-254. https://doi.org/10.1016/j.neuroimage.2012.06.081

Jones, D. K., Knösche, T. R., & Turner, R. (2013). White matter integrity, fiber count, and other fallacies: the do's and don'ts of diffusion MRI. *NeuroImage*, *73*, 239-254.

Katsel, P., Davis, K. L., & Haroutunian, V. (2005). Variations in myelin and oligodendrocyte-related gene expression across multiple brain regions in schizophrenia: A gene ontology study. *Schizophrenia Research*, *79*(2), 157-173. https://doi.org/https://doi.org/10.1016/j.schres.2005.06.007

Keller, D., Erö, C., & Markram, H. (2018). Cell densities in the mouse brain: a systematic review. *Frontiers in neuroanatomy*, *12*, 83.

Koller, K., Rudrapatna, U., Chamberland, M., Raven, E. P., Parker, G. D., Tax, C. M. W., Drakesmith, M., Fasano, F., Owen, D., Hughes, G., Charron, C., Evans, C. J., & Jones, D. K. (2021). MICRA: Microstructural image compilation with repeated acquisitions. *NeuroImage*, *225*, 117406. https://doi.org/https://doi.org/10.1016/j.neuroimage.2020.117406

Kolomeets, N. S., & Uranova, N. A. (2019). Reduced oligodendrocyte density in layer 5 of the prefrontal cortex in schizophrenia. *European Archives of Psychiatry and Clinical Neuroscience*, *269*(4), 379-386. https://doi.org/10.1007/s00406-018-0888-0

Kougioumtzidou, E., Shimizu, T., Hamilton, N. B., Tohyama, K., Sprengel, R., Monyer, H., Attwell, D., & Richardson, W. D. (2017). Signalling through AMPA receptors on oligodendrocyte precursors promotes myelination by enhancing oligodendrocyte survival. *Elife*, *6*. https://doi.org/10.7554/eLife.28080

Le Bihan, D., Mangin, J. F., Poupon, C., Clark, C. A., Pappata, S., Molko, N., & Chabriat, H. (2001). Diffusion tensor imaging: concepts and applications. *Journal of Magnetic Resonance Imaging: An Official Journal of the International Society for Magnetic Resonance in Medicine*, *13*(4), 534-546.

Lee, H., Lee, H.-H., Ma, Y., Eskandarian, L., Gaudet, K., Tian, Q., Krijnen, E. A., Russo, A. W., Salat, D. H., Klawiter, E. C., & Huang, S. Y. (2024). Age-related alterations in human cortical microstructure across the lifespan: Insights from high-gradient diffusion MRI. *Aging Cell*, *23*(11), e14267. https://doi.org/https://doi.org/10.1111/acel.14267

Li, M., Santpere, G., Imamura Kawasawa, Y., Evgrafov, O. V., Gulden, F. O., Pochareddy, S., Sunkin, S. M., Li, Z., Shin, Y., Zhu, Y., Sousa, A. M. M., Werling, D. M., Kitchen, R. R., Kang, H. J., Pletikos, M., Choi, J., Muchnik, S., Xu, X., Wang, D., Lorente-Galdos, B., Liu, S., Giusti-Rodríguez, P., Won, H., de Leeuw, C. A., Pardiñas, A. F., BrainSpan, C., Psych, E. C., Psych, E. D. S., Hu, M., Jin, F., Li, Y., Owen, M. J., O'Donovan, M. C., Walters, J. T. R., Posthuma, D., Reimers, M. A., Levitt, P., Weinberger, D. R., Hyde, T. M., Kleinman, J. E., Geschwind, D. H., Hawrylycz, M. J., State, M. W., Sanders, S. J., Sullivan, P. F., Gerstein, M. B., Lein, E. S., Knowles, J. A., Sestan, N., Willsey, A. J., Oldre, A., Szafer, A., Camarena, A., Cherskov, A., Charney, A. W., Abyzov, A., Kozlenkov, A., Safi, A., Jones, A. R., Ashley-Koch, A. E., Ebbert, A., Price, A. J., Sekijima, A., Kefi, A., Bernard, A., Amiri, A., Sboner, A., Clark, A., Jaffe, A. E., Tebbenkamp, A. T. N., Sodt, A. J., Guillozet-Bongaarts, A. L., Nairn, A. C., Carey, A., Huttner, A., Chervenak, A., Szekely, A., Shieh, A. W., Harmanci, A., Lipska, B. K., Carlyle, B. C., Gregor, B. W., Kassim, B. S., Sheppard, B., Bichsel, C., Hahn, C.-G., Lee, C.-K., Chen, C., Kuan, C. L., Dang, C., Lau, C., Cuhaciyan, C., Armoskus, C., Mason, C. E., Liu, C., Slaughterbeck, C. R., Bennet, C., Pinto, D., Polioudakis, D., Franjic, D., Miller, D. J., Bertagnolli, D., Lewis, D. A., Feng, D., Sandman, D., Clarke, D., Williams, D., DelValle, D., Fitzgerald, D., Shen, E. H., Flatow, E., Zharovsky, E., Burke, E. E., Olson, E., Fulfs, E., Mattei, E., Hadjimichael, E., Deelman, E., Navarro, F. C. P., Wu, F., Lee, F., Cheng, F., Goes, F. S., Vaccarino, F. M., Liu, F., Hoffman, G. E., Gürsoy, G., Gee, G., Mehta, G., Coppola, G., Giase, G., Sedmak, G., Johnson, G. D., Wray, G. A., Crawford, G. E., Gu, G., van Bakel, H., Witt, H., Yoon, H. J., Pratt, H., Zhao, H., Glass, I. A., Huey, J., Arnold, J., Noonan, J. P., Bendl, J., Jochim, J. M., Goldy, J., Herstein, J., Wiseman, J. R., Miller, J. A., Mariani, J., Stoll, J., Moore, J., Szatkiewicz, J., Leng, J., Zhang, J., Parente, J., Rozowsky, J., Fullard, J. F., Hohmann, J. G., Morris, J., Phillips, J. W., Warrell, J., Shin, J. H., An, J.-Y., Belmont, J., Nyhus, J., Pendergraft, J., Bryois, J., Roll, K., Grennan, K. S., Aiona, K., White, K. P., Aldinger, K. A., Smith, K. A., Girdhar, K., Brouner, K., Mangravite, L. M., Brown, L., Collado-Torres, L., Cheng, L., Gourley, L., Song, L., Ubieta, L. D. L. T., Habegger, L., Ng, L., Hauberg, M. E., Onorati, M., Webster, M. J., Kundakovic, M., Skarica, M., Reimers, M., Johnson, M. B., Chen, M. M., Garrett, M. E., Sarreal, M., Reding, M., Gu, M., Peters, M. A., Fisher, M., Gandal, M. J., Purcaro, M., Smith, M., Brown, M., Shibata, M., Brown, M., Xu, M., Yang, M., Ray, M., Shapovalova, N. V., Francoeur, N., Sjoquist, N., Mastan, N., Kaur, N., Parikshak, N., Mosqueda, N. F., Ngo, N.-K., Dee, N., Ivanov, N. A., Devillers, O., Roussos, P., Parker, P. D., Manser, P., Wohnoutka, P., Farnham, P. J., Zandi, P., Emani, P. S., Dalley, R. A., Mayani, R., Tao, R., Gittin, R., Straub, R. E., Lifton, R. P., Jacobov, R., Howard, R. E., Park, R. B., Dai, R., Abramowicz, S., Akbarian, S., Schreiner, S., Ma, S., Parry, S. E., Shapouri, S., Weissman, S., Caldejon, S., Mane, S., Ding, S.-L., Scuderi, S., Dracheva, S., Butler, S., Lisgo, S. N., Rhie, S. K., Lindsay, S., Datta, S., Souaiaia, T., Roychowdhury, T., Gomez, T., Naluai-Cecchini, T., Beach, T. G., Goodman, T., Gao, T., Dolbeare, T. A., Fliss, T., Reddy, T. E., Chen, T., Hyde, T. M., Brunetti, T., Lemon, T. A., Desta, T., Borrman, T., Haroutunian, V., Spitsyna, V. N., Swarup, V., Shi, X., Jiang, Y., Xia, Y., Chen, Y.-H., Jiang, Y., Wang, Y., Chae, Y., Yang, Y. T., Kim, Y., Riley, Z. L., Krsnik, Z., Deng, Z., Weng, Z., Lin, Z., & Li, Z. (2018). Integrative functional genomic analysis of human brain development and neuropsychiatric risks. *Science*, *362*(6420), eaat7615. https://doi.org/10.1126/science.aat7615

Lynch, K. M., Cabeen, R. P., & Toga, A. W. (2024). Spatiotemporal patterns of cortical microstructural maturation in children and adolescents with diffusion MRI. *Hum Brain Mapp*, *45*(1), e26528. https://doi.org/10.1002/hbm.26528

Mancini, M., Karakuzu, A., Cohen-Adad, J., Cercignani, M., Nichols, T. E., & Stikov, N. (2020). An interactive meta-analysis of MRI biomarkers of myelin. *Elife*, *9*, e61523.

Margoni, M., Pagani, E., Preziosa, P., Palombo, M., Gueye, M., Azzimonti, M., Filippi, M., & Rocca, M. A. (2023). In vivo quantification of brain soma and neurite density abnormalities in multiple sclerosis. *Journal of Neurology*, *270*(1), 433-445. https://doi.org/10.1007/s00415-022-11386-3

Margulies, D. S., Ghosh, S. S., Goulas, A., Falkiewicz, M., Huntenburg, J. M., Langs, G., Bezgin, G., Eickhoff, S. B., Castellanos, F. X., Petrides, M., Jefferies, E., & Smallwood, J. (2016). Situating the default-mode network along a principal gradient of macroscale cortical organization. *Proceedings of the National Academy of Sciences*, *113*(44), 12574-12579. https://doi.org/10.1073/pnas.1608282113

Markham, J. A., Morris, J. R., & Juraska, J. M. (2007). Neuron number decreases in the rat ventral, but not dorsal, medial prefrontal cortex between adolescence and adulthood. *Neuroscience*, *144*(3), 961-968. https://doi.org/https://doi.org/10.1016/j.neuroscience.2006.10.015

Miller, D. J., Duka, T., Stimpson, C. D., Schapiro, S. J., Baze, W. B., McArthur, M. J., Fobbs, A. J., Sousa, A. M., Šestan, N., & Wildman, D. E. (2012). Prolonged myelination in human neocortical evolution. *Proceedings of the National Academy of Sciences*, *109*(41), 16480-16485.

Mills, K. L., Goddings, A. L., Herting, M. M., Meuwese, R., Blakemore, S. J., Crone, E. A., Dahl, R. E., Guroglu, B., Raznahan, A., Sowell, E. R., & Tamnes, C. K. (2016). Structural brain development between childhood and adulthood: Convergence across four longitudinal samples. *NeuroImage*, *141*, 273-281. https://doi.org/10.1016/j.neuroimage.2016.07.044

Mournet, S., Okubo, G., Koubiyr, I., Zhang, B., Kusahara, H., Prevost, V. H., Ichinose, N., Triaire, B., Hiba, B., Dousset, V., & Tourdias, T. (2020). Higher b-values improve the correlation between diffusion MRI and the cortical microarchitecture. *Neuroradiology*, *62*(11), 1411-1419. https://doi.org/10.1007/s00234-020-02462-4

Natu, V. S., Gomez, J., Barnett, M., Jeska, B., Kirilina, E., Jaeger, C., Zhen, Z., Cox, S., Weiner, K. S., Weiskopf, N., & Grill-Spector, K. (2019). Apparent thinning of human visual cortex during childhood is associated with myelination. *Proceedings of the National Academy of Sciences*, *116*(41), 20750. https://doi.org/10.1073/pnas.1904931116

Nunez, J. L., Sodhi, J., & Juraska, J. M. (2002). Ovarian hormones after postnatal day 20 reduce neuron number in the rat primary visual cortex. *J Neurobiol*, *52*(4), 312-321. https://doi.org/10.1002/neu.10092

Olesen, J. L., Østergaard, L., Shemesh, N., & Jespersen, S. N. (2022). Diffusion time dependence, power-law scaling, and exchange in gray matter. *NeuroImage*, *251*, 118976. https://doi.org/https://doi.org/10.1016/j.neuroimage.2022.118976

Palombo, M., Ianus, A., Guerreri, M., Nunes, D., Alexander, D. C., Shemesh, N., & Zhang, H. (2020). SANDI: A compartment-based model for non-invasive apparent soma and neurite imaging by diffusion MRI. *Neuroimage*, *215*, 116835. https://doi.org/https://doi.org/10.1016/j.neuroimage.2020.116835

Paquola, C., Bethlehem, R. A. I., Seidlitz, J., Wagstyl, K., Romero-Garcia, R., Whitaker, K. J., Vos de Wael, R., Williams, G. B., Consortium, N., Vértes, P. E., Margulies, D. S., Bernhardt, B., & Bullmore, E. T. (2019). Shifts in myeloarchitecture characterise adolescent development of cortical gradients. *Elife*, *8*, e50482. https://doi.org/10.7554/eLife.50482

Pelvig, D. P., Pakkenberg, H., Stark, A. K., & Pakkenberg, B. (2008). Neocortical glial cell numbers in human brains. *Neurobiology of Aging*, *29*(11), 1754-1762. https://doi.org/https://doi.org/10.1016/j.neurobiolaging.2007.04.013

Peters, A., & Sethares, C. (2004). Oligodendrocytes, their Progenitors and other Neuroglial Cells in the Aging Primate Cerebral Cortex. *Cerebral Cortex*, *14*(9), 995-1007. https://doi.org/10.1093/cercor/bhh060

Petersen, A. C., Crockett, L., Richards, M., & Boxer, A. (1988). A self-report measure of pubertal status: Reliability, validity, and initial norms [journal article]. *J Youth Adolesc*, *17*(2), 117-133. https://doi.org/10.1007/BF01537962

Rajkowska, G., Selemon, L. D., & Goldman-Rakic, P. S. (1998). Neuronal and Glial Somal Size in the Prefrontal Cortex: A Postmortem Morphometric Study of Schizophrenia and Huntington Disease. *Archives of General Psychiatry*, *55*(3), 215-224. https://doi.org/10.1001/archpsyc.55.3.215

Raven, E. P., Veraart, J., Kievit, R. A., Genc, S., Ward, I. L., Hall, J., Cunningham, A., Doherty, J., van den Bree, M. B. M., & Jones, D. K. (2023). In vivo evidence of microstructural hypo-connectivity of brain white matter in 22q11.2 deletion syndrome. *Molecular Psychiatry*. https://doi.org/10.1038/s41380-023-02178-w

Richardson, W. D., Young, K. M., Tripathi, R. B., & McKenzie, I. (2011). NG2-glia as multipotent neural stem cells: fact or fantasy? *Neuron*, *70*(4), 661-673. https://doi.org/10.1016/j.neuron.2011.05.013

Robillard, K. N., Lee, K. M., Chiu, K. B., & MacLean, A. G. (2016). Glial cell morphological and density changes through the lifespan of rhesus macaques. *Brain, behavior, and immunity*, *55*, 60-69. https://doi.org/10.1016/j.bbi.2016.01.006

Satterthwaite, T. D., Shinohara, R. T., Wolf, D. H., Hopson, R. D., Elliott, M. A., Vandekar, S. N., Ruparel, K., Calkins, M. E., Roalf, D. R., Gennatas, E. D., Jackson, C., Erus, G., Prabhakaran, K., Davatzikos, C., Detre, J. A., Hakonarson, H., Gur, R. C., & Gur, R. E. (2014). Impact of puberty on the evolution of cerebral perfusion during adolescence. *Proc Natl Acad Sci U S A*, *111*(23), 8643-8648. https://doi.org/10.1073/pnas.1400178111

Schiavi, S., Palombo, M., Zacà, D., Tazza, F., Lapucci, C., Castellan, L., Costagli, M., & Inglese, M. (2023). Mapping tissue microstructure across the human brain on a clinical scanner with soma and neurite density image metrics. *Human Brain Mapping*, *44*(13), 4792-4811. https://doi.org/https://doi.org/10.1002/hbm.26416

Shirtcliff, E. A., Dahl, R. E., & Pollak, S. D. (2009). Pubertal Development: Correspondence Between Hormonal and Physical Development. *Child Development*, *80*(2), 327-337. https://doi.org/10.1111/j.1467-8624.2009.01263.x

Smith, S. M., Jenkinson, M., Woolrich, M. W., Beckmann, C. F., Behrens, T. E., Johansen-Berg, H., Bannister, P. R., De Luca, M., Drobnjak, I., Flitney, D. E., Niazy, R. K., Saunders, J., Vickers, J., Zhang, Y., De Stefano, N., Brady, J. M., & Matthews, P. M. (2004). Advances in functional and structural MR image analysis and implementation as FSL. *NeuroImage*, *23 Suppl 1*, S208-219. https://doi.org/10.1016/j.neuroimage.2004.07.051

Sydnor, V. J., Larsen, B., Bassett, D. S., Alexander-Bloch, A., Fair, D. A., Liston, C., Mackey, A. P., Milham, M. P., Pines, A., Roalf, D. R., Seidlitz, J., Xu, T., Raznahan, A., & Satterthwaite, T. D. (2021). Neurodevelopment of the association cortices: Patterns, mechanisms, and implications for psychopathology. *Neuron*, *109*(18), 2820-2846. https://doi.org/10.1016/j.neuron.2021.06.016

Sydnor, V. J., Larsen, B., Seidlitz, J., Adebimpe, A., Alexander-Bloch, A. F., Bassett, D. S., Bertolero, M. A., Cieslak, M., Covitz, S., Fan, Y., Gur, R. E., Gur, R. C., Mackey, A. P., Moore, T. M., Roalf, D. R., Shinohara, R. T., & Satterthwaite, T. D. (2023). Intrinsic activity development unfolds along a sensorimotor–association cortical axis in youth. *Nat Neurosci*, *26*(4), 638-649. https://doi.org/10.1038/s41593-023-01282-y

Tamnes, C. K., Herting, M. M., Goddings, A.-L., Meuwese, R., Blakemore, S.-J., Dahl, R. E., Güroğlu, B., Raznahan, A., Sowell, E. R., Crone, E. A., & Mills, K. L. (2017). Development of the Cerebral Cortex across Adolescence: A Multisample Study of Inter-Related Longitudinal Changes in Cortical Volume, Surface Area, and Thickness. *The Journal of Neuroscience*, *37*(12), 3402. https://doi.org/10.1523/JNEUROSCI.3302-16.2017

Tamnes, C. K., Roalf, D. R., Goddings, A. L., & Lebel, C. (2018). Diffusion MRI of white matter microstructure development in childhood and adolescence: Methods, challenges and progress. *Dev Cogn Neurosci*, *33*, 161-175. https://doi.org/10.1016/j.dcn.2017.12.002

Tax, C. M. W., Szczepankiewicz, F., Nilsson, M., & Jones, D. K. (2020). The dot-compartment revealed? Diffusion MRI with ultra-strong gradients and spherical tensor encoding in the living human brain. *NeuroImage*, *210*, 116534. https://doi.org/10.1016/j.neuroimage.2020.116534

Tkachev, D., Mimmack, M. L., Ryan, M. M., Wayland, M., Freeman, T., Jones, P. B., Starkey, M., Webster, M. J., Yolken, R. H., & Bahn, S. (2003). Oligodendrocyte dysfunction in schizophrenia and bipolar disorder. *Lancet*, *362*(9386), 798-805. https://doi.org/10.1016/s0140-6736(03)14289-4

Tournier, J.-D., Smith, R., Raffelt, D., Tabbara, R., Dhollander, T., Pietsch, M., Christiaens, D., Jeurissen, B., Yeh, C.-H., & Connelly, A. (2019). MRtrix3: A fast, flexible and open software framework for medical image processing and visualisation. *NeuroImage*, *202*, 116137.

Vaishnavi, S. N., Vlassenko, A. G., Rundle, M. M., Snyder, A. Z., Mintun, M. A., & Raichle, M. E. (2010). Regional aerobic glycolysis in the human brain. *Proc Natl Acad Sci U S A*, *107*(41), 17757-17762. https://doi.org/10.1073/pnas.1010459107

Velmeshev, D., Perez, Y., Yan, Z., Valencia, J. E., Castaneda-Castellanos, D. R., Wang, L., Schirmer, L., Mayer, S., Wick, B., Wang, S., Nowakowski, T. J., Paredes, M., Huang, E. J., & Kriegstein, A. R. (2023). Single-cell analysis of prenatal and postnatal human cortical development. *Science*, *382*(6667), eadf0834. https://doi.org/10.1126/science.adf0834

Ventura-Antunes, L., Dasgupta, O. M., & Herculano-Houzel, S. (2022). Resting rates of blood flow and glucose use per neuron are proportional to number of endothelial cells available per neuron across sites in the rat brain. *Frontiers in Integrative Neuroscience*, *16*, 821850.

Vijayakumar, N., de Macks, Z. O., Shirtcliff, E. A., & Pfeifer, J. H. (2018). Puberty and the human brain: Insights into adolescent development. *Neuroscience & Biobehavioral Reviews*, *92*, 417-436.

Wagstyl, K., Ronan, L., Goodyer, I. M., & Fletcher, P. C. (2015). Cortical thickness gradients in structural hierarchies. *NeuroImage*, *111*, 241-250. https://doi.org/10.1016/j.neuroimage.2015.02.036

Wannan, C. M., Cropley, V. L., Chakravarty, M. M., Bousman, C., Ganella, E. P., Bruggemann, J. M., Weickert, T. W., Weickert, C. S., Everall, I., & McGorry, P. (2019). Evidence for network-based cortical thickness reductions in schizophrenia. *American Journal of Psychiatry*, *176*(7), 552-563.

Whitaker, K. J., Vértes, P. E., Romero-Garcia, R., Váša, F., Moutoussis, M., Prabhu, G., Weiskopf, N., Callaghan, M. F., Wagstyl, K., Rittman, T., Tait, R., Ooi, C., Suckling, J., Inkster, B., Fonagy, P., Dolan, R. J., Jones, P. B., Goodyer, I. M., the, N. C., Bullmore, E. T., Goodyer, I., Bullmore, E., Dolan, R., Fonagy, P., Jones, P., Fletcher, P., Suckling, J., Weiskopf, N., Fearon, P., Inkster, B., Prabhu, G., Bernal-Casas, D., Eldar, E., Ganguly, T., Hauser, T., Ioannidis, K., Lewis, G., Mita, A., Moutoussis, M., Neufeld, S., Polek-MacDaeid, E., Romero-Garcia, R., St Clair, M., Tait, R., Toseeb, U., van Harmelen, A.-L., Vértes, P., Whitaker, K., Will, G.-J., Ziegler, G., Zimbron, J., Haarsma, J., Davies, S., Griffin, J., Hart, M., Váša, F., Wagstyl, K., Ooi, C., Widmer, B.,

Alrumaithi, A., Birt, S., Cleridou, K., Dadabhoy, H., Firkins, A., Granville, S., Harding, E., Hopkins, A., Isaacs, D., King, J., Knight, C., Kokorikou, D., Maurice, C., McIntosh, C., Memarzia, J., Mills, H., O'Donnell, C., Pantaleone, S., Scott, J., Stribling, A., Bhatti, J., Hubbard, N., Ilicheva, N., Kentell, M., Wallis, B., & Villis, L. (2016). Adolescence is associated with genomically patterned consolidation of the hubs of the human brain connectome. *Proceedings of the National Academy of Sciences*, *113*(32), 9105-9110. https://doi.org/10.1073/pnas.1601745113

Willing, J., & Juraska, J. M. (2015). The timing of neuronal loss across adolescence in the medial prefrontal cortex of male and female rats. *Neuroscience*, *301*, 268-275. https://doi.org/https://doi.org/10.1016/j.neuroscience.2015.05.073

Wood, S. N. (2003). Thin plate regression splines. *Journal of the Royal Statistical Society Series B: Statistical Methodology*, *65*(1), 95-114.

Xu, X., Wells, A. B., O'Brien, D. R., Nehorai, A., & Dougherty, J. D. (2014). Cell type-specific expression analysis to identify putative cellular mechanisms for neurogenetic disorders. *J Neurosci*, *34*(4), 1420-1431. https://doi.org/10.1523/jneurosci.4488-13.2014

Yeo, B. T., Krienen, F. M., Sepulcre, J., Sabuncu, M. R., Lashkari, D., Hollinshead, M., Roffman, J. L., Smoller, J. W., Zöllei, L., Polimeni, J. R., Fischl, B., Liu, H., & Buckner, R. L. (2011). The organization of the human cerebral cortex estimated by intrinsic functional connectivity. *J Neurophysiol*, *106*(3), 1125-1165. https://doi.org/10.1152/jn.00338.2011

Yeung, Maggie S. Y., Zdunek, S., Bergmann, O., Bernard, S., Salehpour, M., Alkass, K., Perl, S., Tisdale, J., Possnert, G., Brundin, L., Druid, H., & Frisén, J. (2014). Dynamics of Oligodendrocyte Generation and Myelination in the Human Brain. *Cell*, *159*(4), 766-774. https://doi.org/https://doi.org/10.1016/j.cell.2014.10.011

Young, K. M., Psachoulia, K., Tripathi, R. B., Dunn, S. J., Cossell, L., Attwell, D., Tohyama, K., & Richardson, W. D. (2013). Oligodendrocyte dynamics in the healthy adult CNS: evidence for myelin remodeling. *Neuron*, *77*(5), 873-885. https://doi.org/10.1016/j.neuron.2013.01.006

Zhang, H., Schneider, T., Wheeler-Kingshott, C. A., & Alexander, D. C. (2012). NODDI: practical in vivo neurite orientation dispersion and density imaging of the human brain [Article]. *NeuroImage*, *61*(4), 1000-1016. https://doi.org/10.1016/j.neuroimage.2012.03.072

Zhou, Z., Wei, D., Liu, W., Chen, H., Qin, S., Xu, P., Zuo, X.-N., Luo, Y.-J., & Qiu, J. (2023). Gene transcriptional expression of cortical thinning during childhood and adolescence. *Human Brain Mapping*, *44*(10), 4040-4051. https://doi.org/https://doi.org/10.1002/hbm.26328